Polyhedron 29 (2010) 463–469

Contents lists available at ScienceDirect

Polyhedron

journal homepage: www.elsevier.com/locate/poly

Mixed-ligand metallosupramolecular complexes with Br_n-terephthalic acid (n = 1 or 4) and a versatile bent dipyridyl tecton: Structural modulation by substituent effect of the ligand and metal ion

Cheng-Peng Li, Jing Chen, Miao Du *

College of Chemistry and Life Science, Tianjin Key Laboratory of Structure and Performance for Functional Molecule, Tianjin Normal University, Tianjin 300387, PR China

ARTICLE INFO

Article history:
Available online 24 June 2009

Keywords:
Metallosupramolecular complex
Crystal structure
Substituent effect
Secondary interaction
In situ ligand reaction

ABSTRACT

This work presents a series of Zn^{II}, Cd^{II}, Co^{II}, and Pb^{II} supramolecular complexes assembled from a bent dipyridyl derivative 2,5-bis(3-pyridyl)-1,3,4-oxadiazole (3-bpo) and different dicarboxyl co-ligands 2-bromoterephthalic acid (H_2BTA) and tetrabromoterephthalic acid (H_2TBTA). All products have been prepared under similar conditions and characterized by IR, microanalysis, and TG–DTA techniques. Single-crystal X-ray diffraction indicates that these complexes display mononuclear, 1-D, and 2-D coordination motifs, and diverse higher-dimensional extended networks are further constructed *via* additional secondary interactions such as H-bonding and aromatic stacking. Notably, *in situ* hydrolysis reaction of 3-bpo is observed in the Pb^{II} complex with H_2TBTA, affording another dipyridyl-type ligand *N*,*N*′-bis(3-picolinoyl)hydrazine (3-bph). These results evidently reveal the significant substituent effect of terephthalic acid in structural direction of these metallosupramolecular systems that are also regulated by the selection of metal ions.

1. Introduction

The flourishing realm of crystal engineering, which focuses on the successful achievement of desired crystalline solids from predesigned bridging ligands and metal ions, has provided a useful and effective synthetic strategy for the construction of functional materials with established and potential applications [1–9]. At present, it has been extensively realized that the deliberate selection and utilization of organic tectons plays a profound role in such metallosupramolecular assemblies [10–15]. In this regard, building components involving pyridyl and/or carboxylate functional groups (for example, 4,4′-bipyridyl and terephthalic acid) have been confirmed to be the most reliable candidates for structural assembly of new coordination solids with interesting network architectures and physicochemical properties [16–30].

In this context, our previous studies on a modified dipyridyl ligand with the oxadiazole spacer, namely 2,5-bis(3-pyridyl)-1,3,4-oxadiazole (3-bpo), have revealed that such a building block may show three typical conformations (see Chart 1), various coordination modes, and potential capability for participating in secondary interactions, which thus result in multifarious metallosupramolecular systems *via* coordinative and other noncovalent contacts [31]. As for the Br-substituted terephthalic acid, 2-bromoterephthalic acid (H_2BTA) has been utilized to synthesize reticular porous metal–organic frameworks with good capacity for gas adsorption [32–34]. And very recently, another related analogous compound, tetrabromoterephthalic acid (H_2TBTA), has also been employed to construct novel coordination networks [35,36], in which the Br-substituents impose a significant steric effect on the formation of such supramolecular architectures. In this contribution, we will present a series of Zn^{II}, Cd^{II}, Co^{II}, and Pb^{II} mixed-ligand complexes based on H_2BTA or H_2TBTA (see Chart 1) incorporated with 3-bpo as the building blocks, aiming to explore the intrinsic steric and electronic effect of the Br-substituent of terephthalic acid on the structural direction of these coordination solids.

2. Experimental

2.1. Materials and general methods

All reagents and solvents were commercially available and used as received. Fourier transform (FT) IR spectra (KBr pellets) were recorded on an AVATAR-370 (Nicolet) spectrometer. Elemental analyses were carried out on a CE-440 (Leemanlabs) analyzer. Thermogravimetric (TG) and differential thermal analysis (DTA) experiments were performed in the temperature range of 25–700 °C on a Rigaku standard TG-DTA analyzer under nitrogen atmosphere at a heating rate of 10 °C/min with an empty Al_2O_3 crucible as the reference.

* Corresponding author. Tel./fax: +86 22 23766556.
E-mail address: dumiao@public.tpt.tj.cn (M. Du).

0277-5387/$ - see front matter © 2009 Elsevier Ltd. All rights reserved.
doi:10.1016/j.poly.2009.06.041

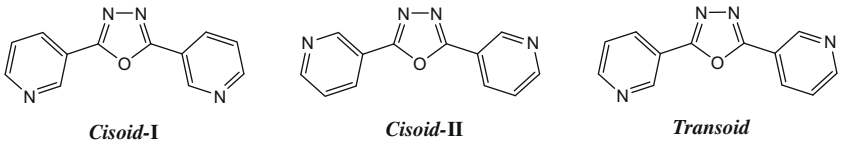

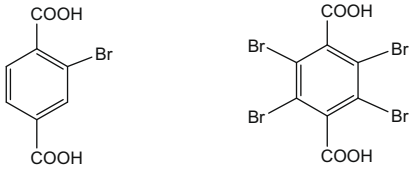

Chart 1.

2.2. Synthesis of complexes **1**–**6**

2.2.1. [Zn(HBTA)$_2$(3-bpo)$_2$](H$_2$O) (**1**)

A mixture of H_2BTA (24.5 mg, 0.1 mmol) and 3-bpo (22.4 mg, 0.1 mmol) was dissolved in DMF/H_2O (10 mL, v/v = 1/1) under stirring, which was placed at the bottom of a straight glass tube. Then, a CH_3OH solution (10 mL) of $Zn(NO_3)_2{\cdot}6H_2O$ (29.7 mg, 0.1 mmol) was carefully layered onto it. Upon evaporation of the solvents, colorless block crystals of **1** suitable for X-ray diffraction were obtained after ca. 1 week in 51% yield (26.0 mg, based on H_2BTA). *Anal.* Calc. for $C_{40}H_{26}ZnN_8O_{11}Br_2$: C, 47.11; H, 2.57; N, 10.99. Found: C, 46.89; H, 2.71; N, 11.12%. IR (cm^{-1}): 3495bs, 1716m, 1623vs, 1549w, 1468m, 1366s, 1296s, 1239s, 1092m, 1044s, 813m, 772w, 726w, 688w, 648w, 536m.

2.2.2. [Cd(HBTA)$_2$(3-bpo)$_2$(H$_2$O)$_2$](H$_2$O)$_3$ (**2**)

The same synthetic method as that for **1** was used except that $Zn(NO_3)_2{\cdot}6H_2O$ was replaced by $Cd(NO_3)_2{\cdot}4H_2O$ (30.8 mg, 0.1 mmol), producing colorless block crystals of **2** after ca. 1 week in 50% yield (28.5 mg, based on H_2BTA). *Anal.* Calc. for $C_{40}H_{34}CdN_8O_{15}Br_2$: C, 42.18; H, 3.01; N, 9.84. Found: C, 41.89; H, 3.34; N, 10.01%. IR (cm^{-1}): 3425bs, 1641vs, 1578vs, 1466m, 1397s, 1328w, 1245w, 1094m, 1047m, 979w, 781m, 693m, 587w, 514w.

2.2.3. {[Zn(TBTA)(3-bpo)$_2$(H$_2$O)$_2$](H$_2$O)$_2$}$_n$ (**3**)

The same synthetic method as that for **1** was used except that H_2BTA was replaced by H_2TBTA (48.2 mg, 0.1 mmol), giving colorless block crystals of **3** after ca. 1 week in 70% yield (37.3 mg, based on 3-bpo). *Anal.* Calc. for $C_{32}H_{24}ZnN_8O_{10}Br_4$: C, 36.07; H, 2.27; N, 10.52. Found: C, 36.20; H, 1.99; N, 10.26%. IR (cm^{-1}): 3352bs, 1582vs, 1470m, 1400s, 1320s, 1196w, 1082m, 1031m, 966w, 870w, 802m, 732m, 696s, 624m, 565m, 525w.

2.2.4. {[Cd(TBTA)(3-bpo)$_2$(H$_2$O)$_2$](H$_2$O)$_2$}$_n$ (**4**)

The same synthetic method as that for **1** was used except that H_2BTA and $Zn(NO_3)_2{\cdot}6H_2O$ were replaced by H_2TBTA (48.2 mg, 0.1 mmol) and $Cd(NO_3)_2{\cdot}4H_2O$ (30.8 mg, 0.1 mmol), respectively. Colorless block crystals of **4** were obtained after ca. 1 week in 62% yield (34.5 mg, based on 3-bpo). *Anal.* Calc. for $C_{32}H_{24}CdN_8O_{10}Br_4$: C, 34.54; H, 2.17; N, 10.07. Found: C, 34.19; H, 2.35; N, 10.24%. IR (cm^{-1}): 3421bs, 1707m, 1596vs, 1462w, 1403m, 1318s, 1241m, 1055s, 782w, 694s, 641w, 561w.

2.2.5. {[Co(TBTA)(3-bpo)$_2$(H$_2$O)$_2$](H$_2$O)$_2$}$_n$ (**5**)

The same synthetic method as that for **1** was used except that H_2BTA and $Zn(NO_3)_2{\cdot}6H_2O$ were replaced by H_2TBTA (48.2 mg, 0.1 mmol) and $Co(OAc)_2{\cdot}4H_2O$ (25.0 mg, 0.1 mmol), respectively. Red block crystals of **5** were obtained after ca. 1 week in 66% yield (35.0 mg, based on 3-bpo). *Anal.* Calc. for $C_{32}H_{24}CoN_8O_{10}Br_4$: C, 36.29; H, 2.28; N, 10.58. Found: C, 35.92; H, 1.98; N, 10.26%. IR (cm^{-1}): 3359bs, 1578vs, 1471m, 1402s, 1320s, 1195w, 1082m, 1031m, 967w, 877w, 801m, 696s, 628w, 566m.

2.2.6. [Pb(TBTA)(3-bph)]$_n$ (**6**)

The same synthetic method as that for **1** was used except that H_2BTA and $Zn(NO_3)_2{\cdot}6H_2O$ were replaced by H_2TBTA (48.2 mg, 0.1 mmol) and $Pb(OAc)_2{\cdot}3H_2O$ (38.0 mg, 0.1 mmol), respectively. Colorless block crystals of **6** were obtained after ca. 2 weeks in 44% yield (40.9 mg). *Anal.* Calc. for $C_{20}H_{10}PbN_4O_6Br_4$: C, 25.85; H, 1.08; N, 6.03. Found: C, 25.61; H, 1.19; N, 5.87%. IR (cm^{-1}): 3435b, 3082m, 1708m, 1608s, 1378vs, 1316vs, 1242m, 1056m, 832w, 785w, 691m, 567w.

2.3. X-ray crystallography

Single-crystal X-ray diffraction data for **1**–**6** were collected on a Bruker Apex II CCD diffractometer at 296(2) K with Mo Kα radiation (λ = 0.71073 Å). There was no evidence of crystal decay during data collection. Semi-empirical absorption corrections were applied using SADABS and the program SAINT was used for integration of the diffraction profiles [37]. The structures were solved by direct methods using the SHELXS program of the SHELXTL package and refined with SHELXL [38]. The final refinement was performed by full-matrix least-squares methods on F^2 with anisotropic thermal parameters for all non-H atoms. In general, hydrogen atoms attached to carbon were generated geometrically and those of oxygen (carboxyl or water) were first located in difference Fourier syntheses and then treated as riding. Isotropic displacement parameters of hydrogen were derived from their parent atoms. Notably, hydrogen atoms of the lattice water molecules of O6 (for **1**) and O8 (for **2**) were not located. In the structure of **4**, the lattice water is disordered over two positions (O5 and O5') with the partial site-occupancies of 0.73 and 0.27, respectively, and the affiliated hydrogen atoms were also not determined. A summary of the crystallographic details of **1**–**6** are shown in Table 1. Selected bond lengths and angles are listed in Table S1 and the hydrogen-bonding geometries are given in Table S2.

3. Results and discussion

3.1. Synthesis and general characterization

All complexes were synthesised by layer-separation diffusion of the DMF/H_2O solution of mixed ligands and the corresponding CH_3OH solution of metal salt at ambient condition, which will

Table 1
Crystallographic data and structural refinement summary for complexes **1–6**.

	1	2	3	4	5	6
Formula	$C_{40}H_{26}ZnN_8O_{11}Br_2$	$C_{40}H_{34}CdN_8O_{15}Br_2$	$C_{32}H_{24}ZnN_8O_{10}Br_4$	$C_{32}H_{24}CdN_8O_{10}Br_4$	$C_{32}H_{24}CoN_8O_{10}Br_4$	$C_{20}H_{10}PbN_4O_6Br_4$
M	1019.88	1138.97	1065.60	1112.63	1059.16	929.15
Crystal size (mm)	0.24 × 0.22 × 0.18	0.25 × 0.24 × 0.23	0.23 × 0.22 × 0.19	0.27 × 0.18 × 0.17	0.22 × 0.16 × 0.14	0.28 × 0.26 × 0.22
Crystal system	monoclinic	monoclinic	triclinic	triclinic	triclinic	monoclinic
Space group	$C2/c$	$P2_1/n$	$P\bar{1}$	$P\bar{1}$	$P\bar{1}$	$C2/c$
a (Å)	32.45(2)	8.9460(4)	8.6257(4)	8.620(1)	8.654(3)	13.651(2)
b (Å)	8.666(5)	15.0761(7)	8.8493(4)	8.969(2)	8.849(3)	11.488(1)
c (Å)	13.997(9)	17.3309(9)	11.5333(5)	11.801(2)	11.528(4)	15.228(2)
α (°)	90	90	89.014(1)	89.238(3)	89.170(5)	90
β (°)	96.32(1)	103.355(1)	84.814(1)	83.345(3)	84.792(5)	105.284(2)
γ (°)	90	90	83.034(1)	81.671(3)	83.096(4)	90
V (Å^3)	3912(4)	2274.2(2)	870.26(7)	896.7(3)	872.8(5)	2303.7(5)
Z	4	2	1	1	1	4
D_{calc} (g·cm^{-3})	1.732	1.663	2.033	2.060	2.015	2.679
μ (mm^{-1})	2.745	2.313	5.369	5.135	5.141	14.309
F(0 0 0)	2040	1136	522	540	519	1712
Parameters	282	305	250	260	250	159
R indices [$I > 2\sigma(I)$]	0.0350, 0.1064	0.0309, 0.0863	0.0234, 0.0599	0.0288, 0.0662	0.0276, 0.0709	0.0287, 0.0733
Goodness-of-fit on F^2	0.982	1.082	1.037	1.041	1.041	1.053

facilitate the slow crystallization of X-ray quality single crystals. In each synthetic case, the equivalent metal/dicarboxyl/dipyridyl ratio was utilized for the starting materials. However, the products were found to have the stoichiometric ratios of 1:2:2 for **1** and **2**, 1:1:2 for **3–5**, and 1:1:1 for **6**. Notably, the dicarboxyl ligand H_2BTA takes the mono-deprotonated form (HBTA) in the resulting complexes **1** and **2**, whereas H_2TBTA is completely deprotonated in **3–6**. Interestingly, *in situ* hydrolysis reaction of 3-bpo occurs during preparation of the Pb^{II} complex **6**, which also represents the first coordination species involving the 3-bph ligand. A related example has been observed in the hydrothermal cocrystallization of 2,5-bis(4-pyridyl)-1,3,4-oxadiazole (4-bpo) with suberic acid [39], which leads to the formation of a binary cocrystal formulated as [suberic acid]·[4-bph] (4-bph = *N*,*N*′-bis(4-picolinoyl)hydrazine).

3.2. Structural analysis of ***1–6***

3.2.1. *[Zn(HBTA)$_2$(3-bpo)$_2$](H$_2$O) (**1**)*

In complex **1**, each Zn^{II} ion is located at a 2-fold axis and takes a tetrahedral coordination geometry provided by two carboxylate oxygen donors from a pair of HBTA anions and two pyridyl nitrogen atoms from a pair of 3-bpo ligands (see Fig. 1a). Weak Zn1···O2 interaction is also found with the distance of 2.876(4) Å. As for 2-bromoterephthalic acid, only one carboxyl group thereof is deprotonated and involved in metal coordination. Interestingly, each 3-bpo adopts the unusual *cisoid*-II conformation and the monodentate ligation mode, which has not been observed in the reported complexes [31]. In this way, a mononuclear coordination motif is formed (see Fig. 1a). As expected, the free carboxyl group of HBTA is hydrogen bonded to the uncoordinated 3-pyridyl group of 3-bpo and thus, each mononuclear molecule is linked to four adjacent ones *via* such O4–H4···N4 interactions to constitute a 2-D (4,4) layer with large rhombic grids, in which the nearest Zn···Zn separation is 20.790 Å (see Fig. 1b left). Three such symmetry-related corrugated layers are entangled in a parallel fashion to result in a 3-fold interpenetrating architecture (see Fig. 1b right). Moreover, the twisty nature of these layers facilitates the recognition sites for aromatic stacking [40] between the phenyl group in HBTA and uncoordinated pyridyl ring in 3-bpo, with the centroid-to-centroid distance and the dihedral angle of ca. 3.6 Å and 4.4°, respectively. As a result, the adjacent 2-D hydrogen-bonding layers are further combined *via* π–π stacking interactions (see Fig. 1c left) to afford a 3-D supramolecular framework of 3-fold interpenetration (see Fig. 1c right).

3.2.2. *[Cd(HBTA)$_2$(3-bpo)$_2$(H$_2$O)$_2$](H$_2$O)$_3$ (**2**)*

Each half-occupied Cd^{II} ion in **2** lying on a symmetric center, is six-coordinated by two pyridyl nitrogen donors as well as four oxygen atoms from two carboxylate groups and two water molecules to furnish an octahedral sphere (see Fig. 2a). A mononuclear coordination motif, which is similar to that in **1**, is also generated in this case. Differently, the incorporation of aqua ligands around the coordination sphere of Cd^{II} leads to the formation of O6–H6B···O4 and O6–H6A···O3 hydrogen bonds with the free oxygen atoms of carboxyl and carboxylate, and thus, a 2-D supramolecular layer (see Fig. 2b) is constructed along the *bc* plane with the adjacent Cd···Cd separation of 11.576 Å. Furthermore, the carboxyl group of HBTA is also hydrogen bonded to the uncoordinated pyridyl segment of 3-bpo and such O5–H5···N4 interactions extend the 2-D layers into a 3-D network (see Fig. 2c). In addition, hydrogen-boning interactions are observed between the lattice water molecule of O7 and the lattice water of O8 as well as the carboxylate group (see Table S2 for details), which may stabilize this 3-D framework. Very small interspace is found in this lattice with a volume of 48.9 Å^3 (2.1% of the unit cell volume).

3.2.3. *{[M(TBTA)(3-bpo)$_2$(H$_2$O)$_2$](H$_2$O)$_2$}$_n$ (M = Zn^{II} for **3**, Cd^{II} for **4**, and Co^{II} for **5**)*

Single-crystal X-ray diffraction reveals that complexes **3–5** are isostructural, hence only the crystal structure of **3** will be discussed in detail here. Each Zn^{II} ion in **3** is located at an inversion center and takes a similar MN_2O_4 octahedral sphere to that in **2** (see Fig. 3a). Notably, the 3-bpo ligand in this structure adopts the *transoid* conformation and unidentate coordination, and only two similar examples have been found in the 23 known metal complexes with 3-bpo [31]. As a result, the adjacent Zn^{II} ions are connected by the TBTA dianionic bridges to afford a 1-D linear chain along [0 0 1] with the Zn···Zn distance of 11.533 Å (see Fig. 3b), which is also decorated by 3-bpo at both sides to form a fishbone-like motif (see Fig. 3c). Each water ligand of O4 is hydrogen bonded (see Fig. 3b) to the adjacent carboxylate within the chain (O4–H4A···O2) and the lattice water molecule around the chain (O4–H4B···O5, see Table S2 for details). These 1-D polymeric motifs are arranged in an interdigitated fashion, which makes the interchain aromatic stacking available to direct a layered network (see Fig. 3c). The centroid-to-centroid distance between the uncoordinated pyridyl group and phenyl ring is ca. 3.6 Å with the dihedral angle of 5.2°. Further investigation of the crystal packing

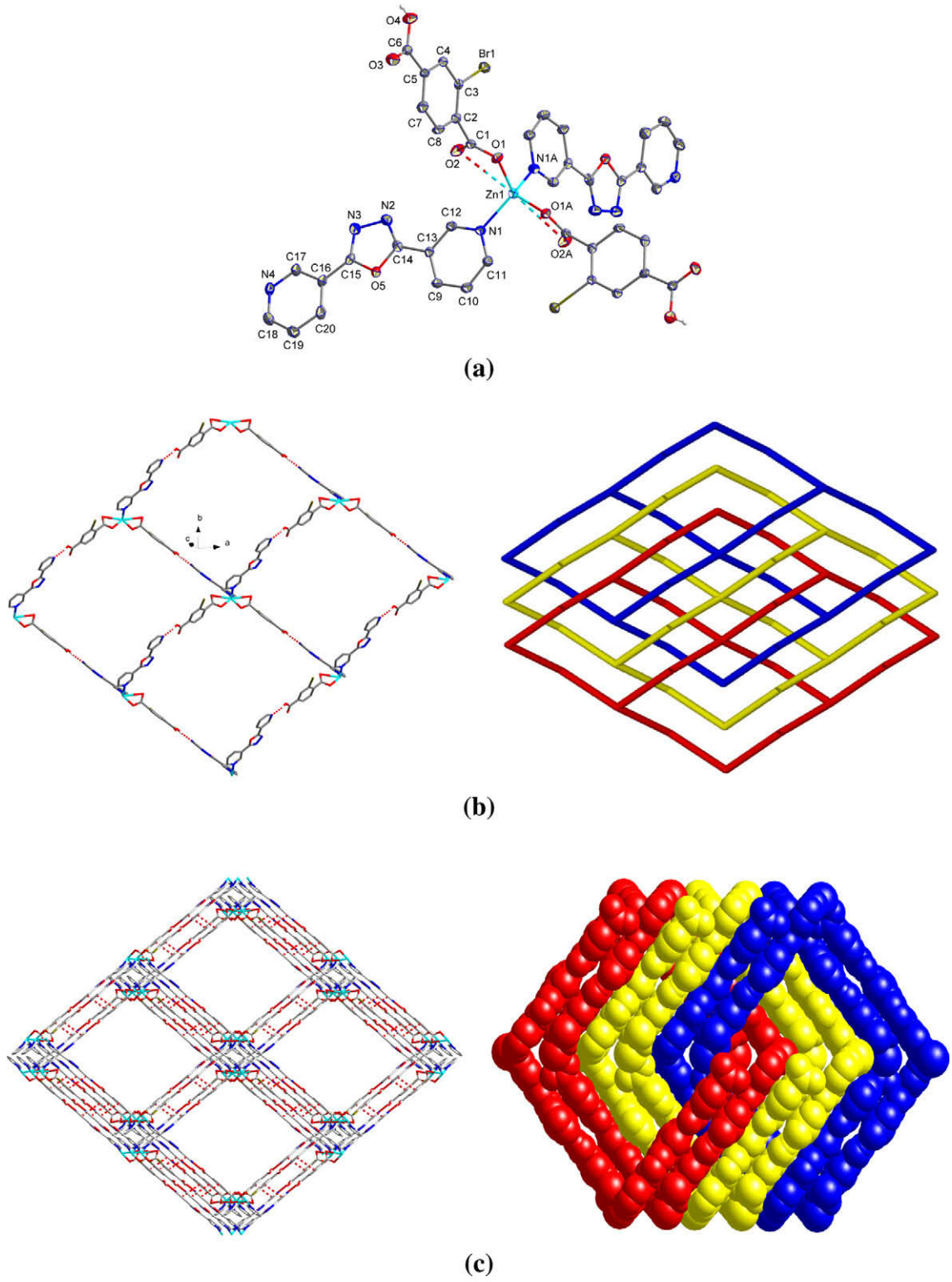

Fig. 1. Views of **1**. (a) ORTEP view (30% thermal ellipsoids) showing the coordination environment of Zn^{II} (symmetry operation for A: $-x, y, -z + 1/2$). (b) (left) Perspective view of the layered H-bonding pattern. (right) Schematic representation of the 3-fold interpenetrating (4,4) layers. (c) (left) 3-D network directed by interlayer aromatic stacking interactions (indicated as red broken lines). (right) Space-filling diagram of the 3-fold interpenetrating 3-D framework.

demonstrates that aromatic stacking interactions are also present between these 2-D patterns, constructing the final 3-D supramolecular lattice (see Fig. 3d). The centroid-to-centroid distance and the dihedral angle between the uncoordinated pyridyl and oxadiazole rings are ca. 3.8 Å and 15.4°, respectively.

3.2.4. *[Pb(TBTA)(3-bph)]$_n$* (***6***)

When the post-transition metal ion Pb^{II} is used in the assembled process, a 2-D coordination polymer is obtained with the observation of *in situ* hydrolysis of the 3-bpo ligand. In this structure, the Pb^{II} center with 2-fold symmetry shows a dis-

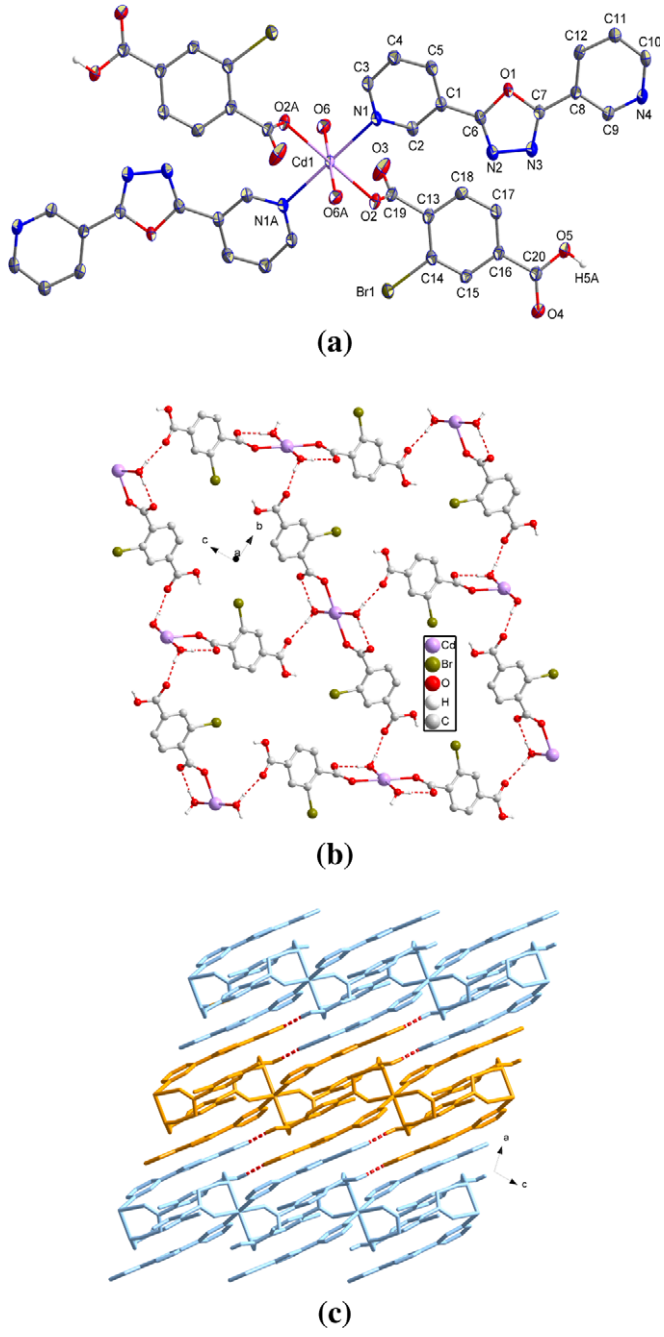

Fig. 2. Views of **2**. (a) ORTEP view (30% thermal ellipsoids) showing the coordination environment of Cd^{II} (symmetry operation for A: $-x$, $-y + 2$, $-z$). (b) Perspective view of the layered network *via* O–H···O interactions between the mononuclear coordination motifs (the 3-bpo ligands are omitted for clarity). (c) 3-D supramolecular lattice *via* additional interlayer O–H···N interactions.

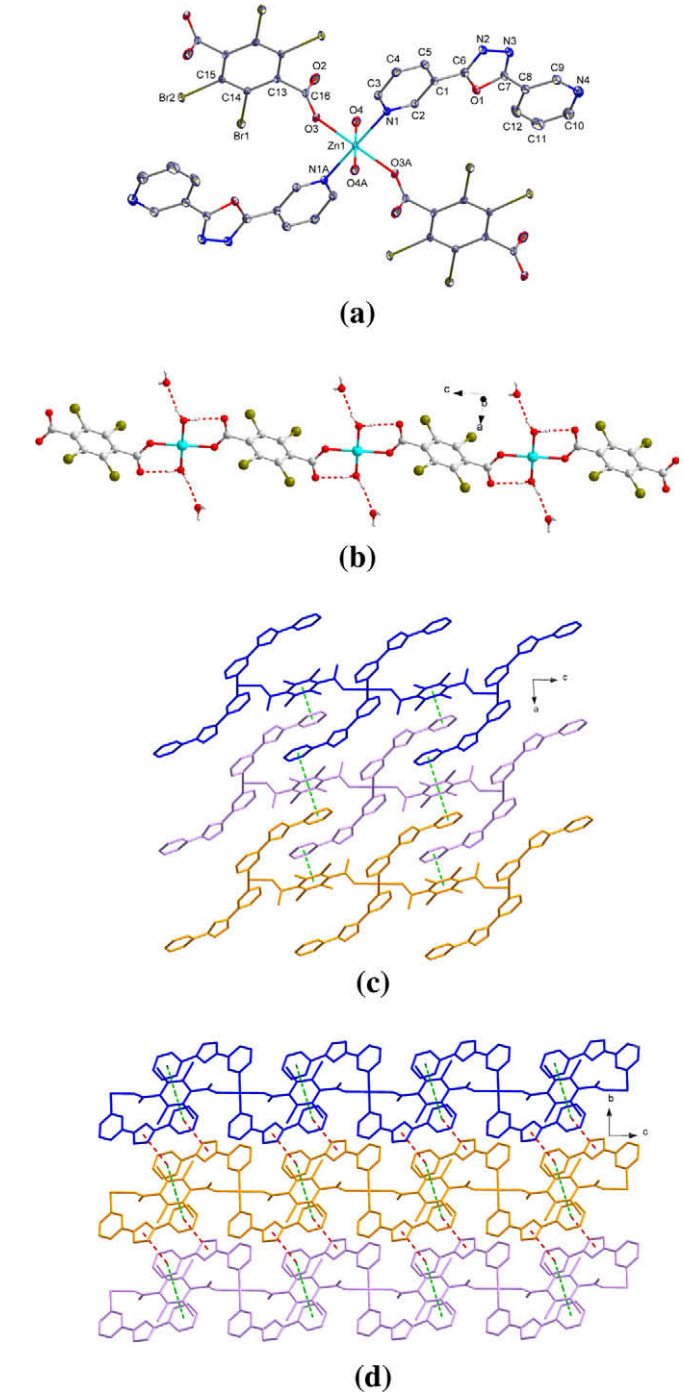

Fig. 3. Views of **3**. (a) ORTEP view (30% thermal ellipsoids) showing the coordination environment of Zn^{II} (symmetry operation for A: $-x + 1$, $-y + 1$, $-z + 1$). (b) Perspective view of the 1-D coordination chain showing the O–H···O bonds (the 3-bpo ligands are omitted for clarity). (c) 2-D supramolecular layer directed by interchain aromatic stacking interactions (indicated as green broken lines). (d) 3-D supramolecular network *via* additional interlayer aromatic stacking interactions (indicated as red broken lines) (For interpretation to the references of color in this figure legend the reader is referred to the web version of the article).

torted octahedral sphere, which is defined by four oxygen atoms from a pair of carboxylate groups and two pyridyl nitrogen donors (see Fig. 4a). Both the *transoid* 3-bph ligands and TBTA dianions serve as bidentate spacers to link the Pb^{II} ions into a (4,4) coordination layer (see Fig. 4b), in which the Pb···Pb separations bridged by 3-bph and TBTA are 13.856 and 11.713 Å, respectively. Such crooked layers align in a parallel mode along [0 1 0], which are further connected by the interlayer N2–H2···O1 bonds (see Table S2) to generate a 3-D supramolecular framework (see Fig. 4c).

3.3. Structural diversity and comparison of ***1*–*6***

In complexes **1**–**6**, a variety of metallosupramolecular architectures with different propagating and packing fashions are constructed, which should be mainly attributed to substituent effect of the dicarboxyl ligand as well as metal ion. It is beneficial to compare their structural features (see Table 2) for further sum-

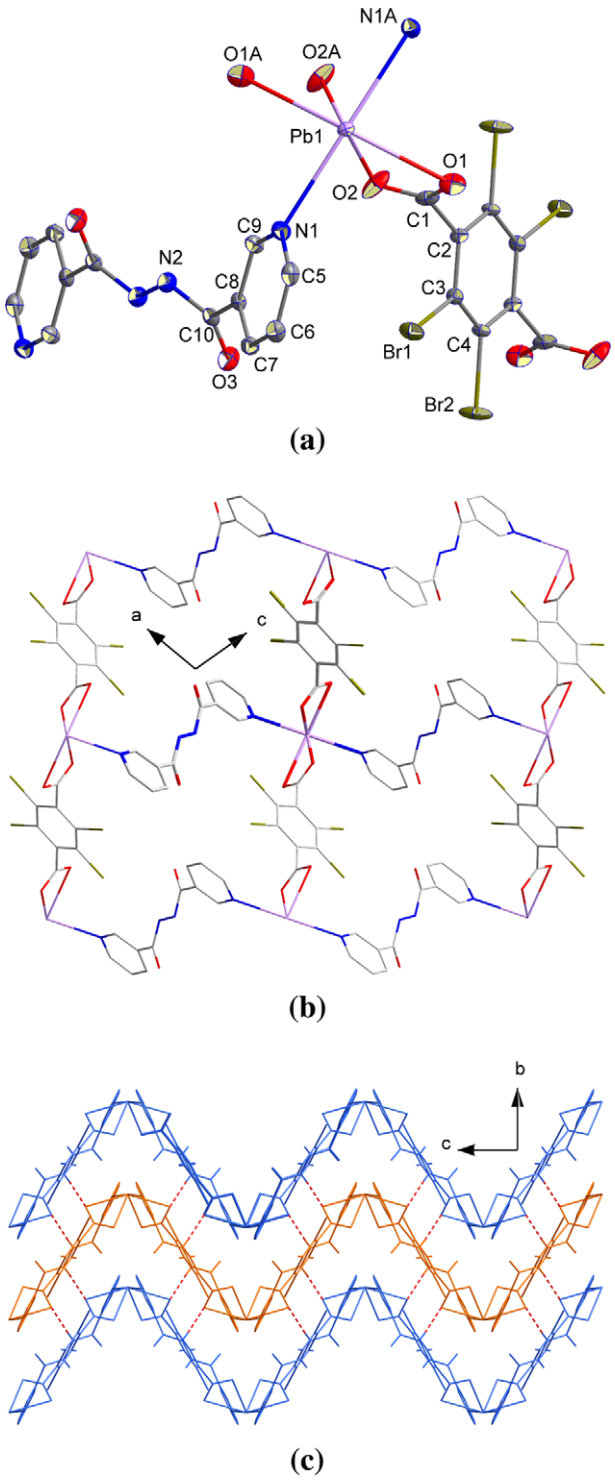

Fig. 4. Views of **6**. (a) ORTEP view (30% thermal ellipsoids) showing the coordination environment of Pb^{II} (symmetry operation for A: $-x, y, -z + 1/2$). (b) Perspective view of the 2-D coordination layer. (c) 3-D supramolecular network *via* interlayer N–H···O interactions.

marizing the role of these impact factors on the assembled processes.

Clearly, although the Br-substituted group is normally regarded as the uncoordinated site, the introduction of different amounts of –Br on the backbone of terephthalic acid (one for H_2BTA and four for H_2TBTA) does significantly affect the deprotonated degree and binding mode of the ligands in their metal complexes. Generally, the Br-substituent can affect the acidity of terephthalic acid in two manners. On the one hand, as an electron-withdrawing group, the Br-substituent can increase the acidity of –COOH by changing its electron density and stabilizing the negatively charged $–COO^-$ counterpart from the viewpoint of field effect, and this effect will decrease when the distance between the –Br and –COOH groups is increased. On the other hand, due to the steric effect, the –COOH group is forced out of the phenyl plane by the *ortho*-Br group to make a nearly perpendicular disposition, and then increases its acidity by adjusting the resonance effect. As a result, by combination of such two types of effects, the acidity of *ortho*-COOH should be stronger than that of the *meta*-COOH in the Br-substituted aromatic dicarboxyl compounds. Accordingly, the two –COOH groups in H_2BTA, locating at the *ortho*- and *meta*-positions to –Br, display different acidity and thus the deprotonated behavior as well as the deviation degree to the Br-substituted phenyl plane in complexes **1** and **2** (see Table 2 for details). And consequently, the –COOH groups of H_2TBTA in the resulting complexes uniformly show the carboxylate form and are nearly perpendicular to the Br_4-substituted phenyl plane (see Table 2).

The nature of metal ion is also a crucial factor in directing the structural assemblage of these complexes. For example, although both the Zn^{II} and Cd^{II} complexes **1** and **2** have the mononuclear coordination motifs with similar binding modes of the ligands, distinct 3-D supramolecular lattices are formed *via* secondary interactions, probably due to their different coordination tendency (the incorporation of additional aqua ligands in **2**). As far as the Zn^{II}, Cd^{II}, and Co^{II} complexes **3**–**5**, the isostructural 1-D coordination arrays should be ascribed to a ligand-directed assembly, while the presence of Pb^{II} ion induces the *in situ* hydrolysis of 3-bpo to afford a 2-D coordination network based on TBTA and 3-bph linkers.

3.4. Thermal stability of *1–6*

All complexes are air stable and their thermal stability was explored by TG-DTA technique (see Fig. S1 for TG–DTA curves). The TG curve of **1** shows the first weight loss of 2.23% (calculated: 1.76%) from 90 to 156 °C, corresponding to the exclusion of one lattice aqua molecule (an endothermic peak at 130 °C in DTA). The residual component starts to decompose until heating to 250 °C, which ends at 616 °C with one endothermic and two exothermic peaks at 263 and 468/543 °C in the DTA curve. As for **2**, the first weight loss of 7.95% from 44 to 139 °C in the TG curve suggests the release of all lattice and coordination water molecules (calculated: 7.90%). Accordingly, one endothermic peak is observed at 132 °C in the DTA curve. Upon further heating to 232 °C, a series of weight losses occur, which end at 588 °C (one endothermic peak at 288 °C and one exothermic peak at 403 °C in DTA). The resulting residue holds a weight of 10.96% of the total sample and seems to be CdO (calculated: 11.27%). Complex **3** is thermally stable to 160 °C, where the weight loss occurs and does not end until heating to 700 °C. Accordingly, one endothermic peak at 223 °C and three exothermic peaks at 249, 451, and 668 °C are observed in the DTA curve. The polymeric framework of **4** is stable up to 120 °C, and then suffers a series of continuous weight losses that end at 690 °C (one endothermic peak at 200 °C and two exothermic peaks at 470/660 °C in DTA). With regard to **5**, the framework remains intact upon heating to 123 °C, followed by a series of weight losses ending at 612 °C (two endothermic peaks at 184/276 °C and one exothermic peak at 468 °C in the DTA curve). The TGA curve of **6** indicates that the coordination network starts to decompose at 178 °C with a sharp weight loss ending at 378 °C. Correspondingly, one endothermic peak and one exothermic peak are observed at 260 and 320 °C in the DTA curve. Further heating of the remaining substance to 700 °C reveals a slow and consecutive weight loss with one exothermic peak appearing at 477 °C in DTA.

Table 2
A comparison of the structural features in complexes **1**–**6**.

Complex	Dicarboxyl	$\theta_{o\text{-}}/\theta_{m\text{-}}$ [a]	Dipyridyl	Hydrogen-bonding	Aromatic stacking
1 (Zn^{II})	HBTA (*o*-COO^-, *m*-COOH)	78.9/7.1	*cisoid*-II-3-bpo	O–H···N	face-to-face
2 (Cd^{II})	HBTA (*o*-COO^-, *m*-COOH)	69.4/12.4	*cisoid*-II-3-bpo	O–H···N/O–H···O	not available
3 (Zn^{II})	TBTA (*o*-COO^-)	80.3/—	*transoid*-3-bpo	O–H···O	face-to-face
4 (Cd^{II})	TBTA (*o*-COO^-)	81.1/—	*transoid*-3-bpo	O–H···O	face-to-face
5 (Co^{II})	TBTA (*o*-COO^-)	80.7/—	*transoid*-3-bpo	O–H···O	face-to-face
6 (Pb^{II})	TBTA (*o*-COO^-)	89.7/—	*transoid*-3-bph	N–H···O	not available

[a] The dihedral angle between the *ortho*-/*meta*-carboxylate/carboxyl group and the Br-substituted phenyl plane.

4. Conclusion

In this work, six new Zn^{II}, Cd^{II}, Co^{II}, and Pb^{II} complexes assembled from the building blocks of Br_n-terephthalic acid and 3-bpo are presented. Their discrete, 1-D, and 2-D coordination motifs are further extended by the secondary interactions to construct diversiform 3-D metallosupramolecular architectures, in which the 3-bpo ligands show unusual *cisoid*-II or *transoid* conformations. Structural diversity of these complexes can be primarily attributed to the significant substituent effect of the Br_n-terephthalic acid tectons as well as the nature of metal ions. These results promote us to make a further systemic study on the coordination chemistry of halogen-substituent dicarboxyl ligands, which may enrich the scope of crystal engineering for supramolecular hybrid solids.

Acknowledgements

This work was financially supported by the National Natural Science Foundation of China (No. 20671071), Program for New Century Excellent Talents in University (No. NCET-07-0613), and Tianjin Normal University.

Appendix A. Supplementary data

CCDC 729695, 729696, 729697, 729698, 729699 and 729700 contain the supplementary crystallographic data for complexes **1**–**6**. These data can be obtained free of charge via http://www.ccdc.cam.ac.uk/conts/retrieving.html, or from the Cambridge Crystallographic Data Center, 12 Union Road, Cambridge CB2 1EZ, UK; fax: (+44) 1223-336-033; or e-mail: deposit@ccdc.cam.ac.uk.

Supplementary data associated with this article can be found, in the online version, at doi:10.1016/j.poly.2009.06.041.

References

[1] B. Moulton, M.J. Zaworotko, Chem. Rev. 101 (2001) 1629.
[2] M.W. Hosseini, Acc. Chem. Res. 38 (2005) 313.
[3] O.R. Evans, W. Lin, Acc. Chem. Res. 35 (2002) 511.
[4] D. Maspoch, D. Ruiz-Molina, J. Veciana, Chem. Soc. Rev. 36 (2007) 770.
[5] G. Férey, Chem. Soc. Rev. 37 (2008) 191.
[6] S. Kitagawa, K. Uemura, Chem. Soc. Rev. 34 (2005) 109.
[7] C. Janiak, Dalton Trans. (2003) 2781.
[8] S.L. James, Chem. Soc. Rev. 32 (2003) 276.
[9] N.W. Ockwig, O. Delgado-Friedrichs, M. O'Keeffe, O.M. Yaghi, Acc. Chem. Res. 38 (2005) 176.
[10] R.-Q. Zou, H. Sakurai, Q. Xu, Angew. Chem., Int. Ed. 45 (2006) 2542.
[11] X.-L. Wang, C. Qin, E.-B. Wang, Z.-M. Su, Y.-G. Li, L. Xu, Angew. Chem., Int. Ed. 45 (2006) 7411.
[12] B.-H. Ye, M.-L. Tong, X.-M. Chen, Coord. Chem. Rev. 249 (2005) 545.
[13] J.-P. Zhang, X.-M. Chen, Chem. Commun. (2006) 1689.
[14] M. Du, Z.-H. Zhang, X.-G. Wang, L.-F. Tang, X.-J. Zhao, CrystEngComm 10 (2008) 1855.
[15] C.-Q. Wan, X.-D. Chen, T.C.W. Mak, CrystEngComm 10 (2008) 475.
[16] M. Fujita, Y.J. Kwon, S. Washizu, K. Ogura, J. Am. Chem. Soc. 116 (1994) 1151.
[17] K. Biradha, M. Sarkar, L. Rajput, Chem. Commun. (2006) 4169, (and reference therein).
[18] X.-L. Wang, C. Qin, E.-B. Wang, L. Xu, Z.-M. Su, C.-W. Hu, Angew. Chem., Int. Ed. 43 (2004) 5036.
[19] S.C. Manna, E. Zangrando, J. Ribas, N.R. Chaudhuri, Dalton Trans. (2007) 1383.
[20] S.S.-Y. Chui, S.M.-F. Lo, J.P.H. Charmant, A.G. Orpen, I.D. Williams, Science 283 (1999) 1148.
[21] N.L. Rosi, J. Kim, M. Eddaoudi, B. Chen, M. O'Keefee, O.M. Yaghi, J. Am. Chem. Soc. 127 (2005) 1504.
[22] K. Barthelet, J. Marrot, D. Riou, G. Férey, Angew. Chem., Int. Ed. 41 (2002) 281.
[23] M. Du, X.-J. Jiang, X.-J. Zhao, Chem. Commun. (2005) 5521.
[24] S. Banerjee, P.-G. Lassahn, C. Janiak, A. Ghosh, Polyhedron 24 (2005) 2963.
[25] B.-L. Chen, K.-F. Mok, S.-C. Ng, M.G.B. Drew, New J. Chem. 23 (1999) 877.
[26] H.-K. Fun, S.S.S. Raj, R.-G. Xiong, J.-L. Zuo, Z. Yu, X.-Z. You, J. Chem. Soc., Dalton Trans. (1999) 1915.
[27] K.-Y. Choi, K.-M. Chun, K.-C. Lee, J. Kim, Polyhedron 21 (2002) 1913.
[28] H.-X. Zhang, B.-S. Kang, A.-W. Xu, Z.-N. Chen, Z.-Y. Zhou, A.S.C. Chan, K.-B. Yu, C. Ren, J. Chem. Soc., Dalton Trans. (2001) 2559.
[29] J. Cano, G.D. Munno, J.L. Sanz, R. Ruiz, J. Faus, F. Lloret, M. Julve, A. Caneschi, J. Chem. Soc., Dalton Trans. (1997) 1915.
[30] H.W. Roesky, M. Andruh, Coord. Chem. Rev. 236 (2003) 91.
[31] M. Du, X.-H. Bu, Bull. Chem. Soc. Jpn. 82 (2009) 539, (and reference therein).
[32] M. Eddaoudi, H. Li, O.M. Yaghi, J. Am. Chem. Soc. 122 (2000) 1391.
[33] M. Eddaoudi, J. Kim, M. O'Keeffe, O.M. Yaghi, J. Am. Chem. Soc. 124 (2002) 376.
[34] M. Eddaoudi, J. Kim, D. Vodak, A. Sudik, J. Wachter, M. O'Keeffe, O.M. Yaghi, Proc. Natl. Acad. Sci. USA 99 (2002) 4900.
[35] C.-P. Li, Y.-L. Tian, Y.-M. Guo, Inorg. Chem. Commun. 11 (2008) 1405.
[36] C.-P. Li, Y.-L. Tian, Y.-M. Guo, Polyhedron 28 (2009) 505.
[37] AXS Bruker, SAINT Software Reference Manual, Madison, WI, 1998.
[38] G.M. Sheldrick, SHELXTL NT Version 5.1. Program for Solution and Refinement of Crystal Structures, University of Göttingen, Germany, 1997.
[39] M. Du, Z.-H. Zhang, X.-J. Zhao, H. Cai, Cryst. Growth Des. 6 (2006) 114.
[40] C. Janiak, J. Chem. Soc., Dalton Trans. (2000) 3885.